Proceedings of the ASME 2021 17th International Manufacturing Science and Engineering Conference
MSEC2022
June 27-July 1, 2022, West Lafayette, Indiana, USA

MSEC2022-85746

AN INVESTIGATION INTO MULTI-TRACK DEPOSITION IN LASER POWDER-BED FUSION: TRANSIENT REGIONS ANALYSIS AND SCAN LENGTH EFFECTS

Santosh Rauniyar[1], Subin Shrestha, Kevin Chou
Additive Manufacturing Institute of Science and Technology
University of Louisville

ABSTRACT

Laser powder bed fusion (L-PBF) additive manufacturing has been used to fabricate complex-shaped structures, which often consist of fine features. Due to transient process phenomena, there are differences in terms of the melt pool formation and the surface morphology depending upon the feature area and scan parameters. This study investigates the scan length effect on the surface morphology and the presence of transient length and width that may have a significant effect as the layer addition continues. For this purpose, four scan lengths (0.25 mm, 0.5 mm, 1.0 mm, and 2.0 mm) are used to fabricate six tracks with back-and-forth scanning. A full factorial design of experiments is used to form multi-track depositions with three levels of power (125 W, 160 W, and 195 W), two levels of scan speed (550 mm/s and 1000 mm/s), and four levels of hatch spacing (80 µm, 100 µm, 120 µm, and 140 µm). A white light interferometer is used to acquire the surface data, and MATLAB is used for surface topographical analysis. The results indicated that the scan length has a significant effect on the surface characteristics. The average height of multi-track deposits increases with the decrease of the scan length. Moreover, the transient length and width can be approximated based on the height variation along both the scan and transverse directions, respectively.

Keywords: Additive manufacturing; Laser powder bed fusion; Surface measurement; Transient region.

1. INTRODUCTION

The laser powder bed fusion (L-PBF) process enables the production of complex metallic parts corresponding to layer by layer information from a computer aided design (CAD) model. Each layer of design information is transferred into a machine in which a laser source will melt a layer of 20–100 µm thick metal powder [1]. The process of melting and solidification continues until all the layer's information is completed and a part is built. The properties of that part are highly dependent on the properties of each layer [2]. The layer is basically the raster pattern followed by the laser source in a line [3]. The study of single tracks provides an understanding of the effect of process parameters on the different metal alloys. The study of multiple single tracks with variation in parameters like laser power and scan speed is helpful in finding the optimum process parameters for an alloy [4].

The LPBF process allows a greater degree of freedom in the design of the parts [5] along with the ability to use high grade metal alloys [6]. Furthermore, recent advancement in this technology has enabled the user to create lightweight high-strength [7] and bio-inspired design structures [8], thin walls [9] that cannot be fabricated by conventional manufacturing processes. Many of these designs can have features with dimensions in the range of 1-2 mm or less. The geometrical accuracy and mechanical properties of these features are different in comparison to the bulk components [10].

The LPBF process involves rapid heating, melting and fluid flow and cooling. There is a complex interaction between the laser and the metallic powder, which is highly affected by the change in process parameters [11] [12]. Wu et al [13] studied the limits of fabricating thin wall structures and explored the factors responsible for the limitations. Tomas et al [14] noticed in their research that the standard stripe scan strategy leads to large deviations in the geometrical accuracy of the thin walled structures. Lu et al [15] studied the warpage in thin-walled structured and concluded that the wall thickness plays an important role on the warpage of the final part. In their study, Yang et al [16] concluded that the longer and taller thin-wall structures are more prone to distortion. The melt pool boundary as well as the microstructures is inconsistent and are not comparable with the bulk components.

The melt pool for long passes will reach a quasi-steady state after the laser beam travels a certain distance provided that the

[1] Contact author: santosh.rauniyar@louisville.edu

scanning direction is unchanged [17]. The melt pool geometry for small scan length exhibits higher variations. Furthermore, the laser beam goes through a phase of acceleration or deceleration at turn points at which the melt pool exhibits different properties [18].

The presence of a transient region at the start and the end of the laser scan is evident for different materials used with the LPBF process [19-21]. The melt pool geometry in the transient region is different from the quasi-steady region. This difference becomes more apparent while building structures with thin features in the LBPF process. Many of the small features do not share the same characteristics as the bulk components even if they are built with the same processing parameters. Also, the surface morphology is affected by the transient regions formed during the back-and-forth scanning. This affects the powder layer thickness across the layer during the next layer deposition, which in turn affects the inter-layer fusion. However, there is a lack of study on how the formation of the transient region affects the surface characteristics of different size features. In this regard, a single-layer multi-track experiment is designed to study the formation of the transient regions during raster scanning. Four scan lengths are fabricated with different levels of laser power, scan speed, and hatch spacing values to define the transient length, width, and examine the length effect on the surface characteristics. The surface data is acquired using a white light interferometer and MATLAB is utilized for further analysis.

2. SAMPLE DESIGN AND FABRICATION

The surface characteristics of the raster scan of 2 mm were analyzed in this study. The raster scans were built with Ti-6AL-4V powder particles. Once the parts were built and removed from the build plate, the raster scan information was captured using a White light interferometer. The data acquired from the raster scans were further processed in Matlab.

An experiment was designed to study the effect of power, scan speed, hatch spacing, and scan length on the residual heat effect in the powder bed fusion process. The experiment was carried out in an EOSINT M 270 metal printer. The machine is equipped with a 200 Watt Continuous wave Ytterbium fiber laser. The laser beam diameter in default conditions is 100 microns. The build was completed with Skywriting ON option. Three levels of power and two levels of scan speed were selected for the experiment. The combination of these power and scan speed produces a continuous track based on the previous experiment of the single tracks [16]. The power and the scan speed along with the linear energy density values is listed in Table 1. Four levels of hatch spacing that allows varying degree of overlap on the subsequent tracks over the range of six different linear energy density were included. Table 2 lists the four levels of hatch spacing and four levels of scan lengths used in the experiment. Ninety-six unique raster scans, as presented in Table 3, were built from the combination of these parameters.

Table 1: Power and scan speed used in the experiment.

	Scan speed (mm/s)	
	550	1000
Power (W)	Linear energy density (J/mm)	
125	0.227	0.125
160	0.291	0.160
195	0.355	0.195

Table 2: Hatch spacing values and scan lengths used in the experiment.

Scan length (mm)	0.25	0.5	1	2
Hatch Spacing (µm)	80	100	120	140

Table 3: Number of levels of parameters

	Power	Scan speed	Scan length	Hatch spacing	Total unique
Level	3	2	4	4	96

A semi-cylindrical design was chosen to build the raster scans at a certain height instead of on the build plate. The intent was to incorporate the variations of the powder distribution in a powder bed fusion process. Twenty-four unique raster scans from three level of power, two levels of scan speed and four levels of scan lengths were arranged on the surface of the semi-cylindrical sample. During the build, one layer of the raster scan was deposited on the top surface of the semi-cylinder. Figure 1 shows the schematic of the arrangement of scans of one hatch spacing case Four semi-cylindrical samples with hatch spacing of 80, 100, 120 and 140 µm were built to include all ninety-six unique scans. All the raster scans were built with six scan lines. Four replicates were built for each hatch spacing case. Figure 2 shows the design and the dimension of a representative sample. The sample has raised wall on either side along the length to avoid any accidental contact during the data acquisition process as well as notches to mark the position of the scans. Furthermore, the laser scan direction along the raster was set up in two distinct ways. In the first method, the laser scanned the six lines of a single raster scan of 0.25 mm scan length and then move onto the scan of six lines of raster scan of 0.5 mm. Whereas in the second method, the laser will scan the first line along the entire length of the samples followed by the second line in the alternating direction. The laser scan direction alternates after each scan, as shown in Figure 3. This will result in higher delay time for the second line of raster scans.

metrological difference between the raster scan of different parameters.

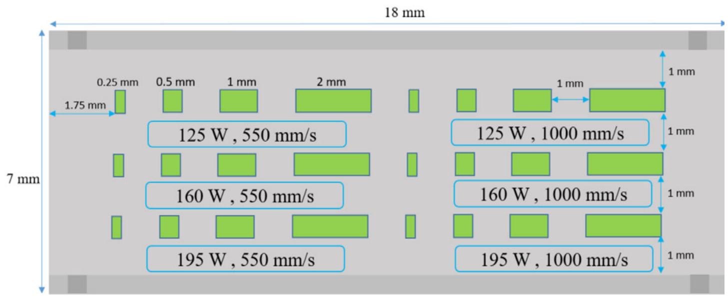

Figure 1: Twenty-four raster scan tracks of four different scan lengths arranged on a semi-cylindrical sample for one hatch spacing case.

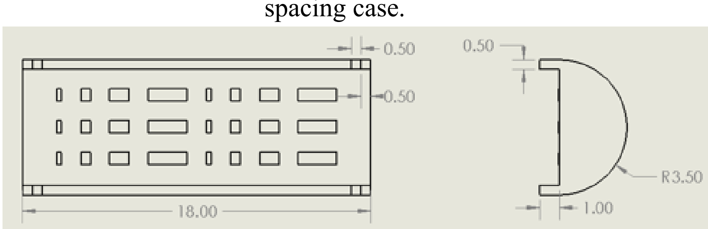

Figure 2: Dimension of the semi- cylindrical sample with twenty-four raster scans (Top, and side view).

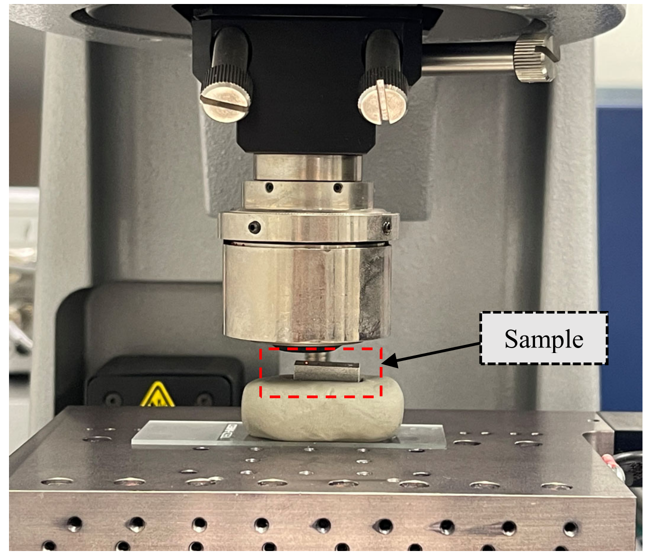

Figure 4. Sample setup for the measurement

3. SURFACE DATA ACQUISITION

A non-contact optical profiler, WYKO NT1100 from Veeco Metrology, was used to acquire the surface data of the raster scans. The instrument was calibrated using a 10 µm step-height standard. Vertical scanning interferometry (VSI) measurement mode was chosen with an objective lens of 50X and a 0.5X field of view lens. This gives an effective field of view of 0.25 mm * 0.19 mm. Therefore, multiple scans had to be done to capture the entire raster area of scan lengths 0.25, 0.5,1, and 2 mm in a single image. The instrument is equipped with a motorized stage for stitching large area measurements. Multiple scans with a back-scan of 250 µm were stitched with a rectangular stitching function to acquire the image of the raster scans. The pixel resolution of the acquired image is approx. 339.5 nm * 396 nm. Figure 4 shows the sample setup for measurements. The output data is saved in the WYKO vision analysis software in the form of .opd file extension. The surface height data can be visualized as well as filtered in the vision software. However, the acquired data showed several powder particulates attached to the surface of the raster scans. The data acquired from the scan was filtered using the combination of Vision software and Matlab code to remove the powder particulate from the raster scans. Gaussian filtering with a high pass filter of 0.2 mm was used in the raw data in the vision software. The initial data and the data passed through a high pass filter was compared in MATLAB to obtain the raster scan data without powder particulates. The voids created due to the removal of particulates was filled with a moving median of 500-700. And the edges were be smoothed using median filtering of 50 in MATLAB. The final output in ASCII format was modified to match the. opd format. The output was imported into the vision software to study the

The optical profiler software provides several options for data filtering. However, selective removal of the powder particles was not possible in one step in the vision software. MATLAB provides more flexibility for data filtering compared to the vision software. The algorithm written in MATLAB was successful in removing the powder particulates and smoothing out the surface height data. The surface height for six lines on the raster scan for all parameter cases was analyzed after importing the filtered data into the vision software. Figure 5 shows an example of the raw data obtained from the scan in the optical profiler. The image consists of one data point at every 339.46 nm in the x-direction and 396.05 nm in the y-direction. This sample image has total of 7371 columns and 2783 rows of data points representing the surface height. The black dots on the image are the bad pixel points where the scan could not generate data. The data for those points is filled by using an interpolation of measurement data. An example of the data restored by using surrounding 35-pixel points is presented in Figure 6. Furthermore, the contrast between the tracks and the particulates is observed after the use of a high pass Gaussian filter as shown in Figure 7.

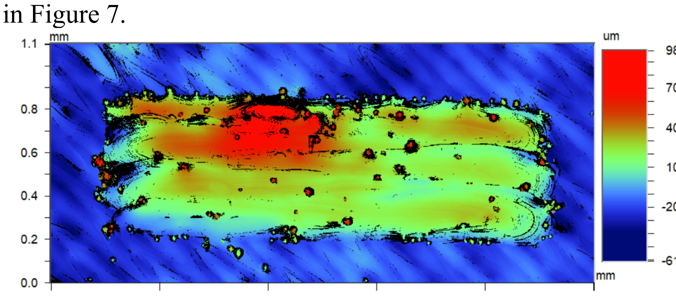

Figure 5: Top view of the sample of raw data visualized in the vision software.

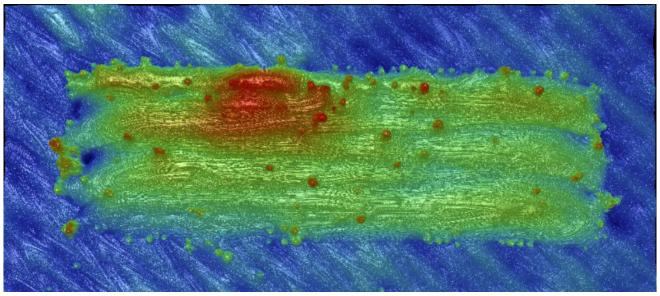

Figure 6. Rendered data after restoring the bad pixel points.

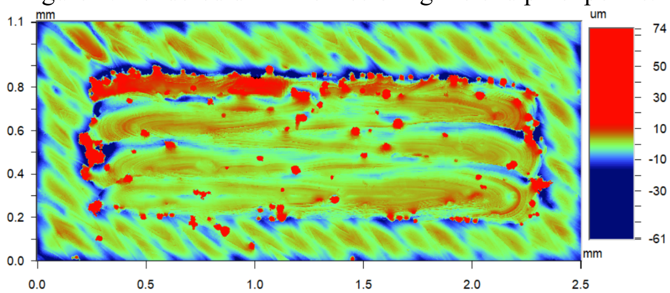

Figure 7: Example of high pass Gaussian filtering to contrast the powder particulates.

4. DATA SMOOTHING AND FILTRATION

The fabricated multi-tracks consist of randomly distributed powder particles and spatters attached to the surface which affects the surface comparison. Hence, the powder particles are removed to compare the surface statistics. Moreover, the region of interest, in this case, is the six tracks. The six-track region is separated from the substrate, which is the previous layer deposition for the analysis and comparison.

4.1 Smoothing powder particles

The surface data is passed through a high pass Gaussian filtering of 0.2 mm. The original surface data and the filtered data is contrasted in MATLAB. A user written code compares the two data and removes the higher surface height using a cutoff value. Figure 8 shows the surface data without powder particles plotted in MATLAB. The missing data is filled with a moving median of 500 elements. However, some data spikes are present around the powder particles. To remove the spikes, a third-order one-dimensional median filter of length 50 is applied to the entire data set. The final filtered and smoothed data is shown in Figure 9. This data is then imported into the Vision software for further analysis.

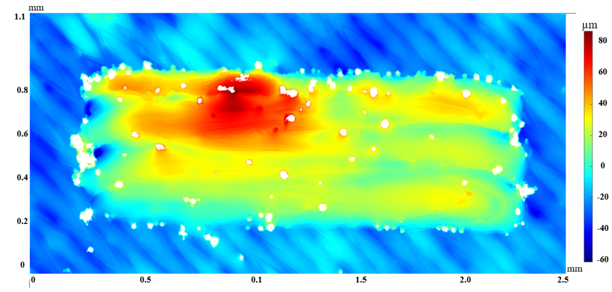

Figure 8: This figure shows the data removed from the powder particles.

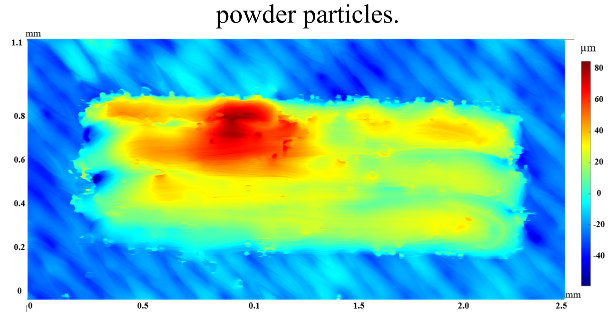

Figure 9: Surface height data without the powder particles.

4.2 Separating multi-track area from the previous layer data

The multi-track region scanned using the white light interferometer consists of the previous/substrate layer data, which is considered as background in this study. Hence, the background data is removed for the analysis and comparison between different cases. The transition between the two layers is distinct as highlighted in Figure 10, which is used as a criterion to separate the six multi-tracks from the background using a MATLAB code.

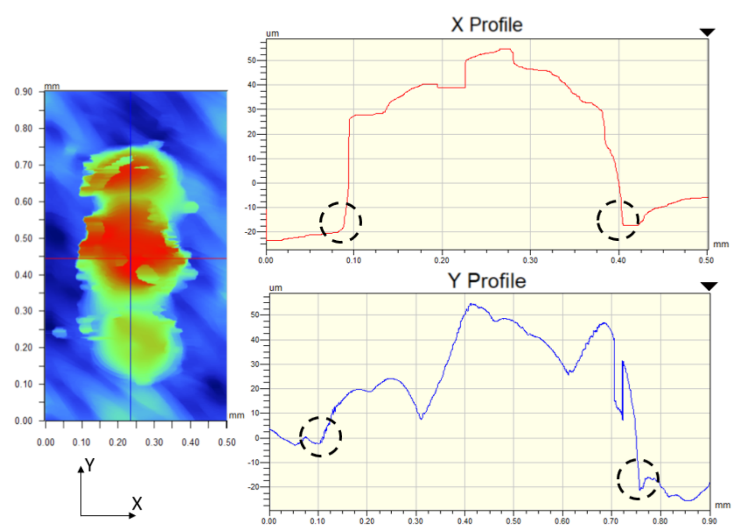

Figure 10: Characteristic used to separate the multi-track region from the background**.**

Four points p1, p2,p3, and p4 are defined, and the search is performed to find the maximum slope for all rows and columns. After identifying the multitrack region based on the slope, the background is then assigned a Nan value. Figure 11 shows the separation of the multitrack region from the background for scan lengths of 0.25 mm.

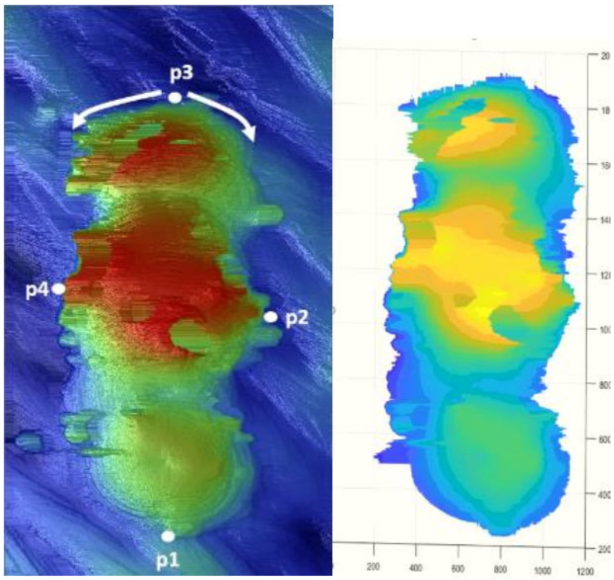

Figure 11: Multi-track region isolated from the background using MATLAB for a typical case (125 W laser power, 550 mm/s scan speed, 100 µm hatch spacing, and 0.25 mm scan length).

5. RESULTS AND DISCUSSION

5.1 Length effect on surface characteristics.

After separating the multi-track region, the average area roughness is calculated from all the multi-track data. Figure 12 presents the average area roughness along with the standard deviation from four replicates. The effect of laser power, scan speed, and scan length is evident for the 80 µm hatch spacing. In general, the average roughness decreased with increasing scan length, while the roughness increased with increasing power. When the hatch spacing is increased, the trend is not obvious.

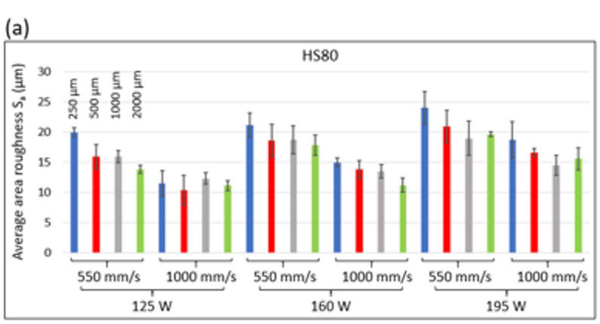

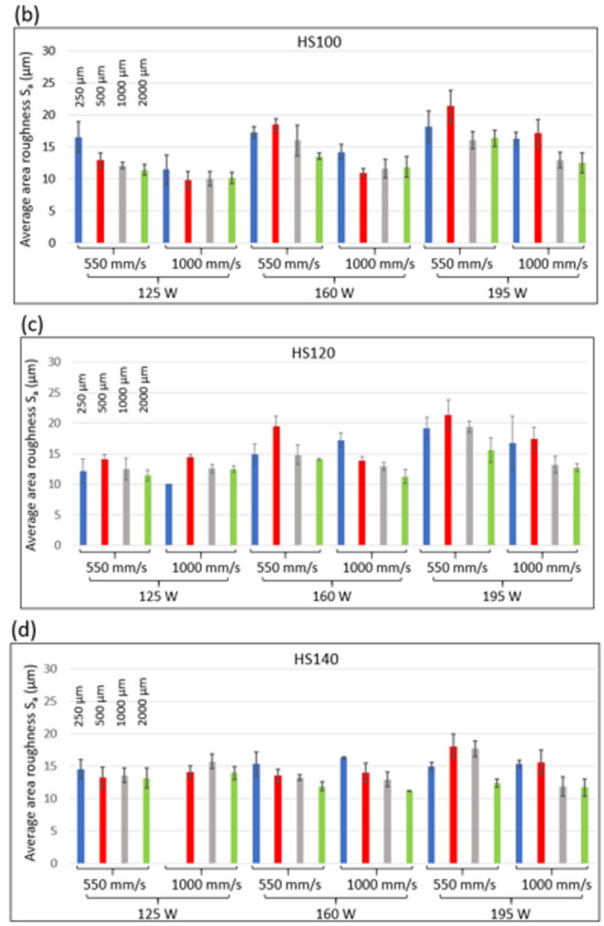

Figure 12: Average area roughness at different hatch spacing values: (a) 80 µm, (b) 100 µm, (c) 120 µm, and (d) 140 µm.

The response of the roughness value due to the four different factors was analyzed using the General linear Model in ANOVA with a confidence limit of 95%. The effect of individual factors and their interactions up to 3 levels on the Ra was studied. All four factors have a significant effect on the Ra, based on their zero p-values. The main effects plot shown in Figure 13 indicates that an increase in the power maximizes the Ra value while the trend is opposite for the other three factors. However, the hatch spacing (HS) value of 120 µm does not follow the trend. It shows that the Ra value for HS 80 µm will have the highest surface roughness. But HS 120 µm will have higher roughness compared to the HS 100 µm and the HS 140 µm.

The roughness is measured from the six tracks including the transient region. The main effect plot shows that the multi-track roughness is higher for the smaller area with high power and low speed. Single track study showed that the transient length is higher for higher power and lower speed. Thus the result obtained with multi-track provides evidence that the roughness in the multi-track is affected by the formation of transient regions.

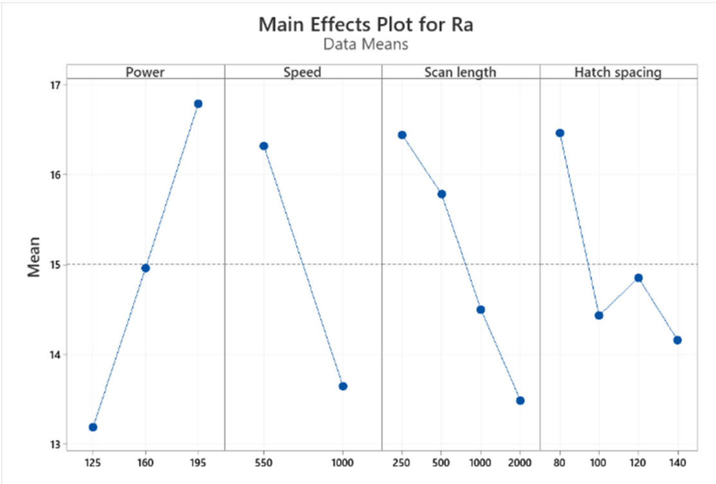

Figure 13: Main effect of four factor to the Ra value

The statistical analysis showed the significance of the transient region on the surface roughness of the multi-tracks. The single-track experiment showed that the difference in surface height between transient and steady regions is noticeable [18]. Therefore, the height based comparison is performed. The average transverse height is obtained for all the cases, and Figure 14 shows the average height profile along the scan direction for four different scan lengths (195 W laser power, 550 mm/s scan speed, and 80 µm hatch spacing). The area profile shows that the surface is elevated at the center for 0.25 mm and 0.5 mm scan length. However, the elevated surface is present at the two edges in the longer scan lengths. It is also interesting to see that for the majority of the cases, the average height is higher for lower scan lengths. The height of the multi-track would significantly affect the magnitude of the mechanical interaction with the recoater blade during the recoating process. Due to the increased height with smaller feature sizes, the interaction force may be higher, which would only increase the chance of build failure.

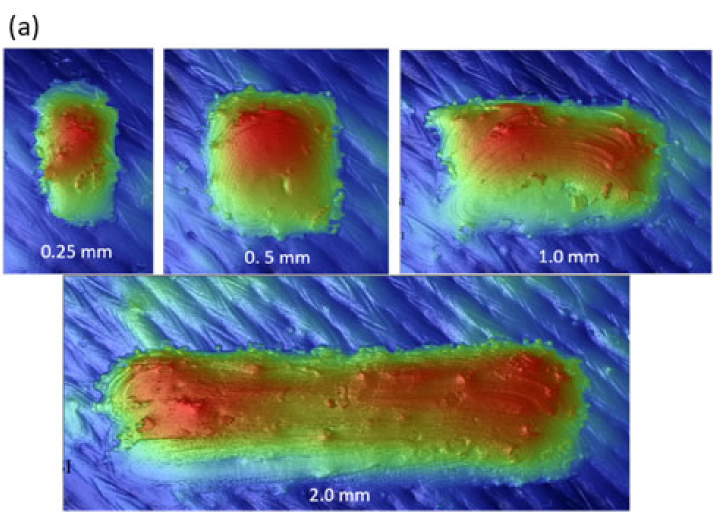

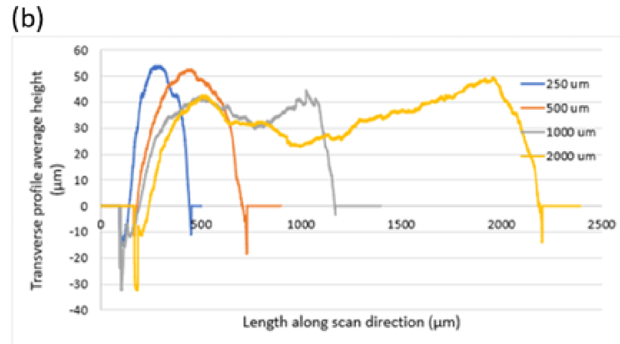

Figure 14: (a) Top view and (b) transverse average height along scan direction from 195 W laser power, 550 mm/s scan speed and 80 µm hatch spacing.

Besides the transient region in the scan direction, the presence of transient region along the transverse direction is also of interest for the multi-track. The surface height along the transverse direction is used to identify the transient width. Figure 15 shows the top view of the 2 mm long multi-tracks formed with 125 W laser power, 550 mm/s scan speed, and 100 µm hatch spacing. The average height of the longitudinal profiles along the transverse direction is obtained. The error bar indicates the standard deviation. The standard deviation is less than 0.5 for all the profiles.

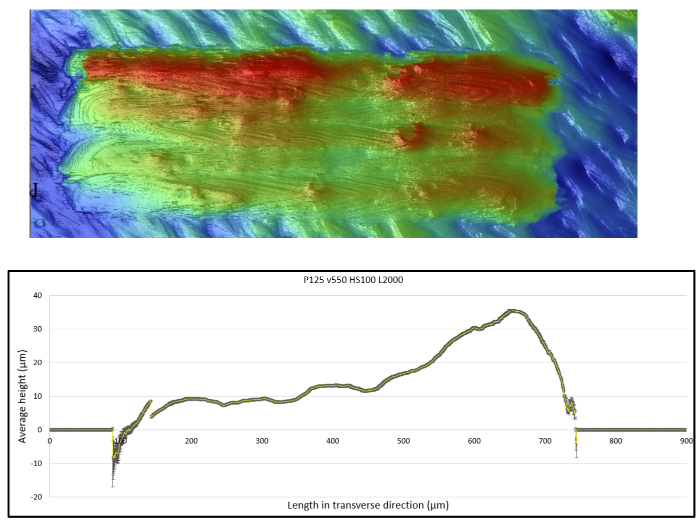

Figure 15: Top view of the multitrack and the average height profile obtained from P125 v550 HS100 and L2000.

Figure 16 shows the average height profiles from all six power and scan speed combinations with 120 µm hatch spacing. One of the profiles, with the lowest energy density, resulted in a wavy profile. This is due to the presence of a gap between the tracks.

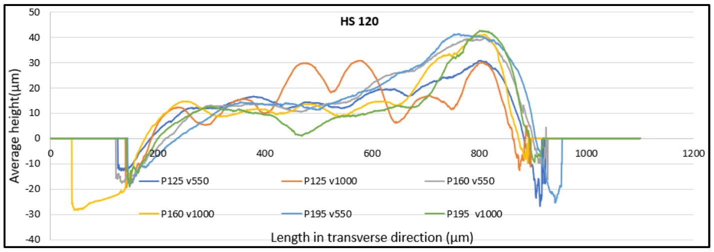

Figure 16: Average height profile along transverse direction with 120 µm hatch spacing.

Figure 17 presents the top view from all six power and scan speed combinations with 140 µm hatch spacing. Figure 18 presents the average height profiles for those cases. In the case of higher hatch spacing, there are more profiles which shows waviness. The tracks with insufficient overlap are removed and the remaining plots are shown in Figure 19.

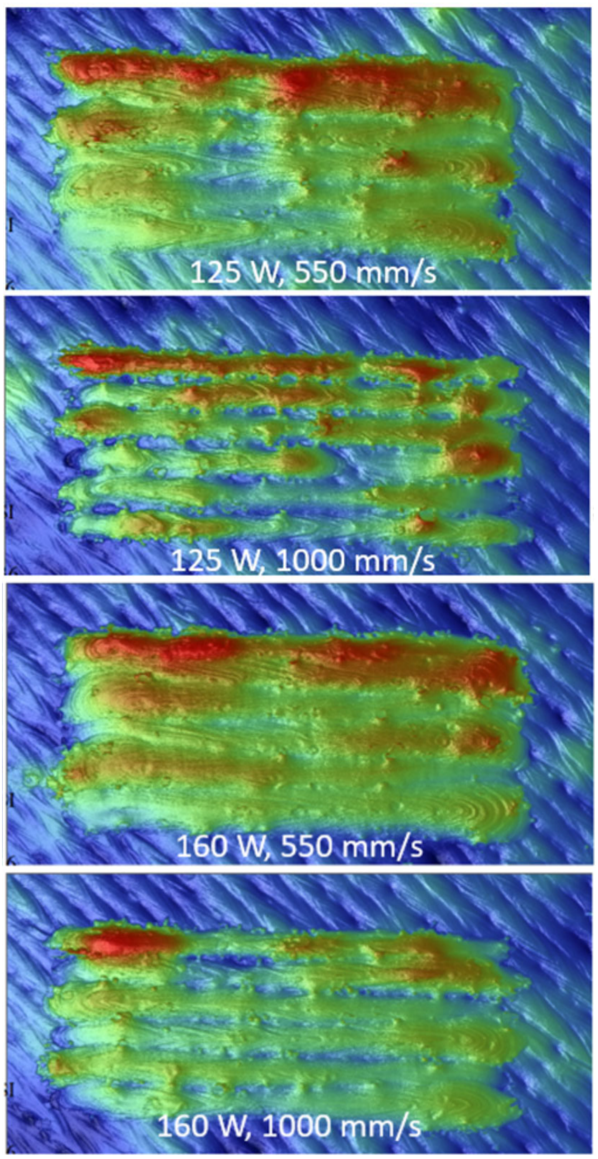

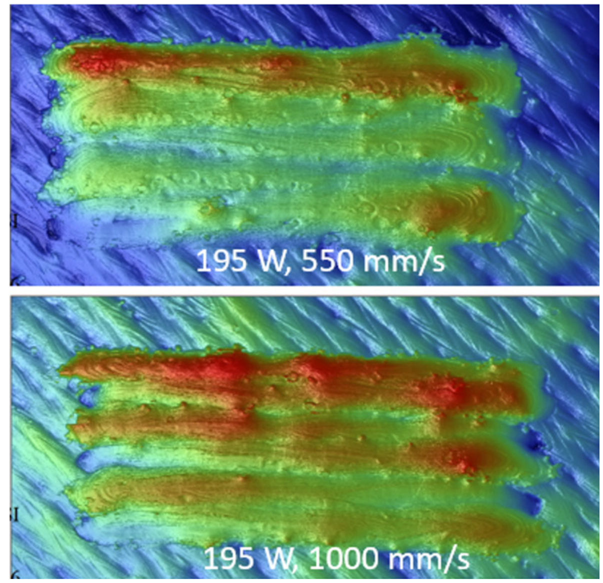

Figure 17: Top view of the multitrack with six power and scan speed combination and a hatch spacing of 140 µm.

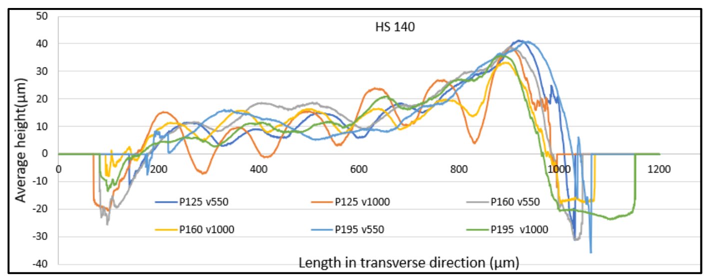

Figure 18: The average height profile obtained with 140 µm hatch spacing.

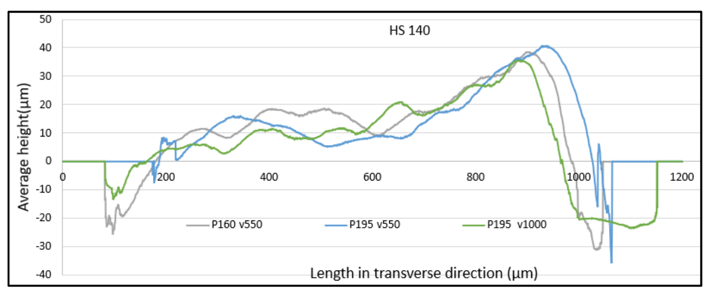

Figure 19: Average height profile after removing cases with insufficient overlap between the tracks.

5.2 Defining transient region in multi-track.

The surface analysis of the multi-tracks showed the presence of transient region in both scan direction and transverse direction. Hence, two terminologies are defined to separate between the transient regions in two directions.

Transient length: The transient region formed along the scan direction is defined as the transient length. The transient length is formed due to the lower initial thermal state of the powder bed. The transient length is higher for higher energy density[1]. Figure 20 shows the top view and the average height profile along the scan direction for a typical single-track case. The transient length is identified based on the height. For this case, the transient length is approximately 600 µm.

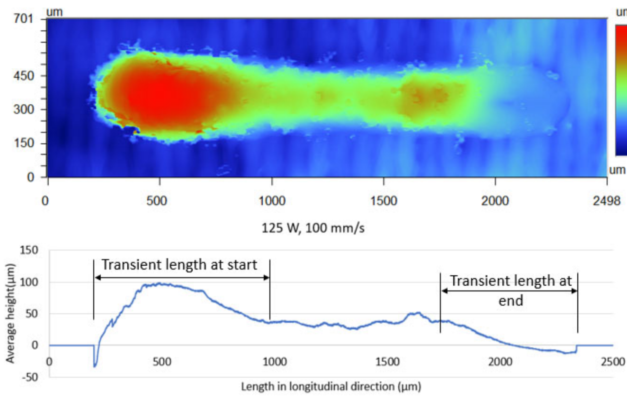

Figure 20: Single track transient length

During the back-and-forth multi-track scanning, the transient length observed at the start of laser and end of laser interact together. Hence, the severity of the transiency is reduced at the two ends as shown in Figure 21.

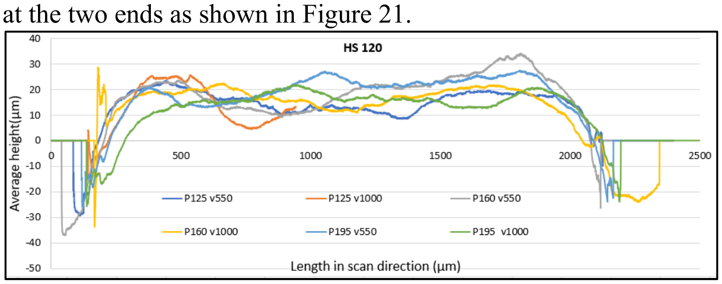

Figure 21: Back and forth scanning leads to similar transient region at two ends.

Transient width: The transient region formed along the transverse direction is called transient width in this study. The transient width exists as the surface height of the first track is the maximum which significantly affects the track morphology of the subsequent tracks. The transient width depends on the combination of laser power, scan speed, and hatch spacing. Figure 22 shows a typical case with distinct transition from the transient to quasi steady state based on the average height profile.

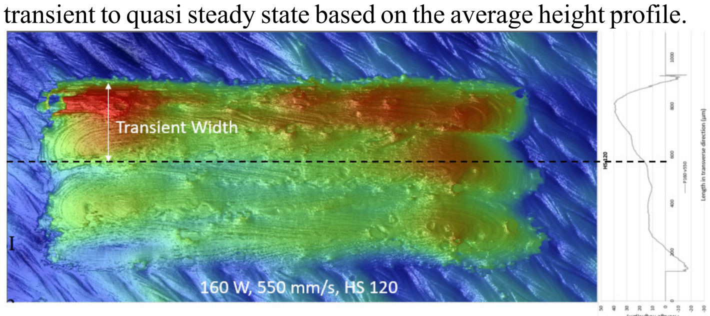

Figure 22: Defining the transient width based on the average height.

Figure 23 shows that the transient width depends on the hatch spacing. The average heigth did not show the steadiness with lower hatch spacing of 80 µm upto six tracks, which suggested that the steady state may reach at higher track number. The results indicated that the width of the multi-track region may be limited to further analyze the transient width for lower hatch spacing values. Therefore, a new experiment was designed to include multiple number of tracks for lower hatch spacings.

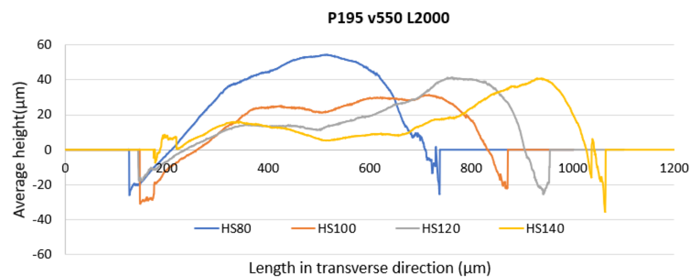

Figure 23: Average height profiles with different hatch spacing values.

Measuring the trasient width: An experiement was performed with a raster scan area of 4 mm * 2 mm instead of the six lines raster scan. Two levels of power 160 W and 195 W, two levels of scan speed 550 mm/s and 1000 mm/s and three levels of hatch spacing 80 µm, 100 µm and 120 µm was selected for the scans. The surface data was acquired as mentioned in the section 3. And, the data smoothing mentioned in the sub section 4.1 was used to remove the powder particles. Figure 24 shows one of the typical result after the removal of powder particles and the surface height variation along the width of the raster scans in the center. The transient width along the y-axis is defined as the starting positing of the track and the lowest surface height. An example of defining the trasient width is shown in Figure 25. The transient width of the twelve paramter combinations was calcualted. The process was repeated for two replicate sets. Table 4 lists the trasient width for two replicate sets. ANOVA analysis of the data shows that the trasient width is affected by all three main parameters i.e., power, scan speeed and the hatch spacing. The main effect plot, presented in Figure 26, shows that higher value of power, higher value of scan speed and higher value of hatch spacing leads to the maximum trasient width.

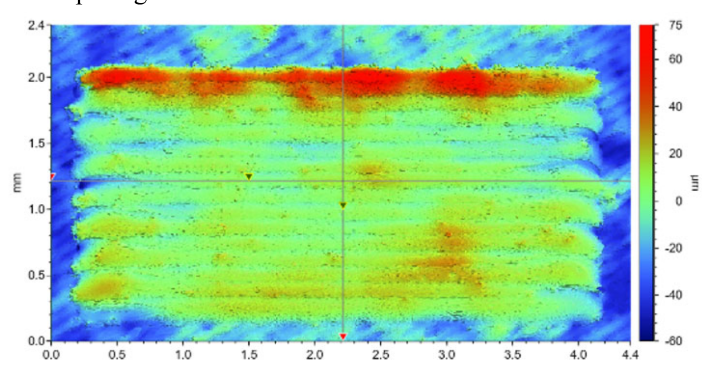

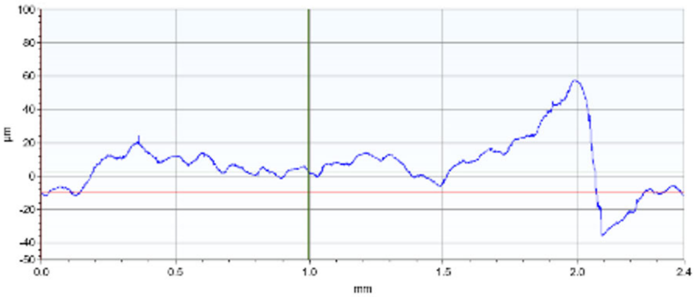

Figure 24: Typical result of 4 mm * 2 mm raster scan and surface height variation along the width of the raster scan

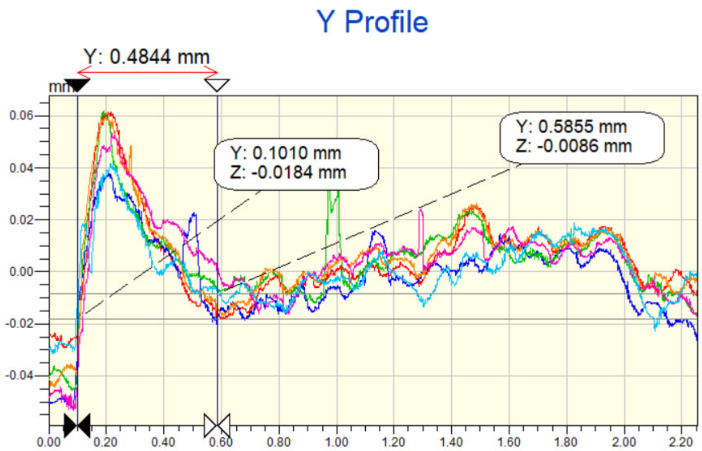

Figure 25: Snapshot of the surface height variation at multiple points along the y-axis

Table 4: Transient width for the twelve parameter combinations

Power (W)	Scan speed (mm/s)	Hatch Spacing (microns)	Transient width (microns)	
			Replicate 1	Replicate 2
160	550	80	340	364
160	1000	80	484	574
195	550	80	464	475
195	1000	80	698	615
160	550	100	371	442
160	1000	100	548	431
195	550	100	429	382
195	1000	100	773	675
160	550	120	624	594
160	1000	120	807	823
195	550	120	680	674
195	1000	120	856	777

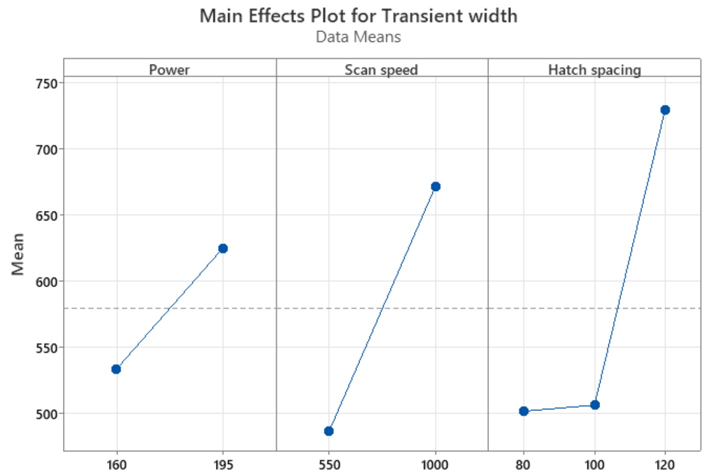

Figure 26: Main effect plots of power, scan speed and hatch spacing on the transient width

6 CONCLUSION

This study focuses on identifying the transient regions and investigating its influence on the surface characteristics of the multi-tracks fabricated using the LPBF process. Six back and forth tracks are fabricated using different levels of laser power (125 W, 160 W and 195 W), scan speeds (550 mm/s and 1000 mm/s), hatch spacing (80 µm, 100 µm, 120 µm, and 140 µm), and scan lengths (0.25 mm. 0.5 mm, 1 mm, and 2 mm). The surface formed with different parameters are measured using a white light interferometer and the results and analyses lead to following conclusions:

1. The geometry of the tracks on the raster scans vary along the scan direction as well as the transverse direction. The surface height can be used as a measure to distinguish the transient region and quasi steady state region.
2. The parameters that resulted in larger transient region also resulted in higher surface roughness. The shorter scan lengths which only consisted of transient zone resulted in higher surface roughness. The main effect plot showed that increasing the scan length reduced the average roughness.
3. Transient width is highly affected by the hatch spacing. The transient width could not be identified for lower hatch spacing values as the result showed the quasi-steady state may not have reached over the investigated number of tracks.
4. Large area experiment showed that the transient width is higher for the higher power of 195 W, higher scan speed of 1000 mm/s, and the higher hatch spacing value of 120 microns.

ACKNOWLEDGEMENT

This research is partially supported by NSF, Advanced Manufacturing Program (Award # 1921263**).**

REFERENCES

[1] Wang, D., Yang, Y., Su, X. & Chen, Y. Study on energy input and its influences on single-track, multi-track, and multi-layer in SLM. Int. J. Adv. Manuf. Technol. 58, 1189–1199 (2012).

[2] I. Yadroitsev, A. Gusarov, I. Yadroitsava, I. Smurov, Single track formation in selective laser melting of metal powders, J. Mater. Proc. Technol., 210, 1624-1631 (2010)

[3] Dilip, J. J. S., Anam, A., Pal, D. & Stucker, B. A short study on the fabrication of single track deposits in SLM and characterization. Solid Free. Fabr. Symp. 1644–1659 (2016).

[4] Gaikwad A, Giera B, Guss GM, Forien JB, Matthews MJ, Rao P. Heterogeneous sensing and scientific machine learning for quality assurance in laser powder bed fusion – A single-track study. Addit Manuf. 2020;36:101659. doi:10.1016/J.ADDMA.2020.101659

[5] Liu B, Wildman R, Tuck C, Ashcroft I, Hague R. Investigaztion the effect of particle size distribution on processing parameters optimisation in selective laser melting process. 22nd Annu Int Solid Free Fabr Symp - An Addit Manuf Conf SFF 2011. 2011;(January):227-238.

[6] Sing SL, Yeong WY. Laser powder bed fusion for metal additive manufacturing: perspectives on recent developments. Virtual Phys Prototyp. 2020;15(3):359-370. doi:10.1080/17452759.2020.1779999/

[7] du Plessis, A., Yadroitsava, I., and Yadroitsev, I., 2018, "Ti6Al4V Lightweight Lattice Structures Manufactured by Laser Powder Bed Fusion for Load-Bearing Applications," Opt. Laser Technol., 108, pp. 521–528.

[8] Lin, K., Yuan, L., and Gu, D., 2019, "Influence of Laser Parameters and Complex Structural Features on the Bio-Inspired Complex Thin-Wall Structures Fabricated by Selective Laser Melting," J. Mater. Process. Technol., 267(November 2018), pp. 34–43.

[9] Calignano, F., Cattano, G., and Manfredi, D., 2018, "Manufacturing of Thin Wall Structures in AlSi10Mg Alloy by Laser Powder Bed Fusion through Process Parameters," J. Mater. Process. Technol., 255(February), pp. 773–783.

[10] Yang, L., Gong, H., Dilip, S., and Stucker, B., 2014, "An Investigation of Thin Feature Generation in Direct Metal Laser Sintering Systems," Proc. 26th Annu. Int. Solid Free. Fabr. Symp., pp. 714–731.

[11] Bidare, P., Bitharas, I., Ward, R. M., Attallah, M. M., and Moore, A. J., 2018, "Fluid and Particle Dynamics in Laser Powder Bed Fusion," Acta Mater., 142, pp. 107–120.

[12] Matthews, M. J., Guss, G., Khairallah, S. A., Rubenchik, A. M., Depond, P. J., and King, W. E., 2017, "Denudation of Metal Powder Layers in Laser Powder-Bed Fusion Processes," Addit. Manuf. Hand b. Prod. Dev. Def. Ind., 114, pp. 677–693

[13] Wu Z, Narra SP, Rollett A. Exploring the fabrication limits of thin-wall structures in a laser powder bed fusion process. Int J Adv Manuf Technol. 2020;110(1-2):191-207. doi:10.1007/S00170-020-05827-4/FIGURES/14

[14] Tomas J, Hitzler L, Köller M, et al. The dimensional accuracy of thin-walled parts manufactured by laser-powder bed fusion process. J Manuf Mater Process. 2020;4(3). doi:10.3390/JMMP4030091

[15] Lu X, Chiumenti M, Cervera M, Tan H, Lin X, Wang S. Warpage analysis and control of thin-walled structures manufactured by laser powder bed fusion. Metals (Basel). 2021;11(5). doi:10.3390/met11050686

[16] Yang T, Xie D, Yue W, Wang S, Rong P, Shen L, Zhao J, Wang C. Distortion of Thin-Walled Structure Fabricated by Selective Laser Melting Based on Assumption of Constraining Force-Induced Distortion. Metals. 2019; 9(12):1281. https://doi.org/10.3390/met9121281

[17] Scipioni Bertoli, U., Wolfer, A. J., Matthews, M. J., Delplanque, J. P. R., and Schoenung, J. M., 2017, "On the Limitations of Volumetric Energy Density as a Design Parameter for Selective Laser Melting," Mater. Des., 113, pp. 331–340.

[18] Martin, A. A., Calta, N. P., Khairallah, S. A., Wang, J., Depond, P. J., Fong, A. Y., Thampy, V., Guss, G. M., Kiss, A. M., Stone, K. H., Tassone, C. J., Nelson Weker, J., Toney, M. F., van Buuren, T., and Matthews, M. J., 2019, "Dynamics of Pore Formation during Laser Powder Bed Fusion Additive Manufacturing," Nat. Commun., 10(1), pp. 1–10.

[19] Rauniyar, S. and K. Chou. Transient Melt Pool Formation in Laser-Powder Bed Fusion Process. in ASME 2020 15th International Manufacturing Science and Engineering Conference. 2020. American Society of Mechanical Engineers Digital Collection.

[20] Shrestha, S. and K. Chou, A study of transient and steady-state regions from single-track deposition in laser powder bed fusion. Journal of Manufacturing Processes, 2021. 61: p. 226-235.

[21] Bertoli, U.S., et al., On the limitations of volumetric energy density as a design parameter for selective laser melting. Materials & Design, 2017. 113: p. 331-340.

